Slope Diffraction of a Two-Dimensional Dipole Field by a Perfectly Conducting Wedge

Ludger Klinkenbusch and Giuliano Manara

Abstract – The relevance and accuracy of the slope-diffracted field contributions in the uniform geometrical theory of diffraction (UTD) have been studied using a two-dimensional dipole source illuminating a perfectly conducting wedge. Such a two-dimensional dipole source consists of two infinitesimally separated anti-phased line sources that produce a field with a maximum amplitude and no slope in one direction and a maximum slope and no amplitude (null) in the perpendicular direction. The asymptotic numerical results obtained by UTD, including the ordinary and the slope-diffracted contributions, are successfully compared to the exact multipole results for different angles of incidence at different distances from the edge.

1. Introduction

In the high-frequency regime, one of the main advantages of resorting to a ray description of electromagnetic wave propagation in complex scenarios consists of the possibility of determining the distribution of the field in the chosen scenario by a vector summation of the field contributions associated with the rays that, launched at the source point, can reach the observation point by following the laws of both geometrical optics (GO) and the geometrical theory of diffraction (GTD) [1]. In particular, when applying a uniform asymptotic solution as, for example, the uniform geometrical theory of diffraction (UTD) [2], the diffracted field is accurate if the incident field at the diffraction object exhibits a slow spatial variation of its amplitude on a plane perpendicular to the direction of propagation of the correspondent ray. If the field illuminating the scattering object is not slowly varying, then a higher-order term, normally referred to as the slope diffraction term, must be added to the pertinent ray contribution. This problem has been reported in UTD, for example, in the framework of edge diffraction [2, 3] in the two- and the three-dimensional cases.

The purpose of this article is to discuss the relevance and accuracy of the UTD slope-diffracted terms by a comparison with a rigorous solution obtained through a multipole expansion method. This will also allow to provide a set of numerical data able to give evidence to some interesting physical effects, also demonstrating the importance of slope-diffracted contributions in the evaluation of the field under specific illumination conditions. Parts of the contents of this article have been presented in [4].

Manuscript received 18 December 2022.

Ludger Klinkenbusch is with Kiel University, Kaiserstr. 2, D-24143 Kiel, Germany; e-mail: klinkenbusch@tf.uni-kiel.de.

Giuliano Manara is with the University of Pisa, Via G. Caruso 16, I-56122 Pisa, Italy; e-mail: giuliano.manara@unipi.it.

2. Formulation and Exact Solution of the Two-Dimensional Boundary-Value Problem

The geometry of the boundary-value problem is depicted in Figure 1. Two electric or magnetic line sources with equal but anti-phased electric or magnetic current amplitudes are separated by $\mathbf{d}$ and located at $\mathbf{R}' + \mathbf{d}/2$ and $\mathbf{R}' - \mathbf{d}/2$. For the case $|\mathbf{d}| \ll R'$, we call this source configuration a two-dimensional electric or magnetic dipole. This two-dimensional dipole illuminates a perfectly electric conducting (PEC) wedge, as shown in Figure 1. Clearly, if for the angle of the dipole rotation φ_d in Figure 1, $\varphi_d = \varphi'$ holds, the resulting incident field at the edge of the wedge has a maximum amplitude and no slope, whereas for the case $\varphi_d = \varphi' \pm \pi/2$, the incident field at the edge has no amplitude and a maximum slope. For all other values of φ_d, the incident field at the edge consists of both an amplitude and a slope. Such behavior renders the two-dimensional dipole source a perfect candidate for investigating the influence of slope diffraction on the field scattered by the edge of the wedge.

For the phasors (time factor $\exp(j\omega t)$) of the exact total field in plane polar coordinates (R, φ) with $x = R\cos\varphi$ and $y = R\sin\varphi$, we simply superpose the multipole expansions of the fields produced by each of the line sources (see [6, eqs. (11-205) and (11-206)]) and obtain the multipole expansion for E_z (the TM case) and H_z (the TE case) according to

$$\begin{aligned}\begin{matrix}E_z\\H_z\end{matrix}(\mathbf{R}) = \begin{matrix}A_{TM}\\A_{TE}\end{matrix}\frac{1}{\beta}\times\\ \left\{\sum_{n=0}^{\infty}\varepsilon_n H^{(2)}_{\frac{n\pi}{\beta}}(kR_{1,>})J_{\frac{n\pi}{\beta}}(kR_{1,<})\begin{matrix}\sin(\frac{n\pi}{\beta}\varphi)\sin(\frac{n\pi}{\beta}\varphi_1)\\ \cos(\frac{n\pi}{\beta}\varphi)\cos(\frac{n\pi}{\beta}\varphi_1)\end{matrix}\right.\\ \left.-\sum_{n=0}^{\infty}\varepsilon_n H^{(2)}_{\frac{n\pi}{\beta}}(kR_{2,>})J_{\frac{n\pi}{\beta}}(kR_{2,<})\begin{matrix}\sin(\frac{n\pi}{\beta}\varphi)\sin(\frac{n\pi}{\beta}\varphi_2)\\ \cos(\frac{n\pi}{\beta}\varphi)\cos(\frac{n\pi}{\beta}\varphi_2)\end{matrix}\right\}\end{aligned} \tag{1}$$

Here, the wave number k is related to wavelength λ by $k = 2\pi/\lambda$, $\mathbf{R}_1 = \mathbf{R}' + \mathbf{d}/2$, $\mathbf{R}_2 = \mathbf{R}' - \mathbf{d}/2$, and $R_{1,>} = \max(R_1, R)$, $R_{1,<} = \min(R_1, R)$, $R_{2,>} = \max(R_2, R)$, and $R_{2,<} = \min(R_2, R)$. Moreover, A_{TM} and A_{TE} are constants related to the amplitudes I_e and I_m of the each $+z$-directed electric and magnetic line current, as given by

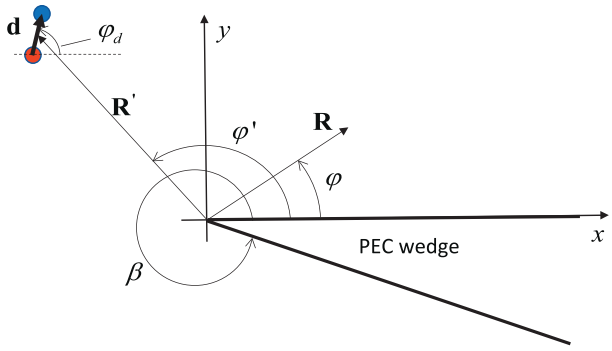

Figure 1. Geometry of the two line sources illuminating a PEC wedge.

$$A_{TM} = -\frac{\pi\omega\mu I_e}{2} \tag{2}$$

$$A_{TE} = -\frac{\pi\omega\epsilon I_m}{2}, \tag{3}$$

J_v and $H_v^{(2)}$ are Bessel functions of the first kind and Hankel functions of the second kind, respectively, each of order v, and

$$\varepsilon_n = \begin{cases} 2 & \text{if } n = 1, 2, \ldots \\ 1 & \text{if } n = 0 \end{cases} \tag{4}$$

3. High-Frequency Asymptotic Solution

According to the GTD [1] or its extension, the UTD [7], the high-frequency asymptotic solution for E_z or H_z of the problem sketched in Figure 1 consists of the GO field (i.e., the direct field E_z^i or H_z^i, which is the incident electric or magnetic field in regions that are optically visible from the source point, and the reflected field E_z^r or H_z^r) plus the diffracted field E_z^d or H_z^d. According to [6], the diffracted field may include both a contribution that is proportional to the amplitude of the incident field at the edge and an additional contribution that is proportional to the normal derivative with respect to the direction of propagation (slope) of the incident field at the edge. For $|\mathbf{d}| \ll R_1$, we thus have

$$E_z^d(\mathbf{R}) = \left[E_z^i|_{R=0} D_s + \frac{1}{jk}\frac{\partial E_z^i}{\partial n}\bigg|_{R=0} \frac{\partial D_s}{\partial \varphi'}\right]\sqrt{\frac{R'}{R'+R}}e^{-jkR} \tag{5}$$

and

$$H_z^d(\mathbf{R}) = \left[H_z^i|_{R=0} D_h + \frac{1}{jk}\frac{\partial H_z^i}{\partial n}\bigg|_{R=0} \frac{\partial D_h}{\partial \varphi'}\right]\sqrt{\frac{R'}{R'+R}}e^{-jkR}, \tag{6}$$

respectively. Here, D_s and D_h represent the ordinary UTD diffraction coefficients for the soft (Dirichlet) and hard (Neumann) cases, while the UTD slope diffraction coefficients are denoted by $\frac{\partial D_s}{\partial \varphi'}$ and $\frac{\partial D_h}{\partial \varphi'}$, respectively [6].

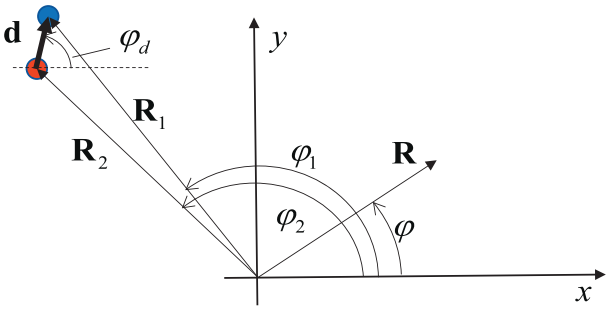

Figure 2. Two line sources forming a two-dimensional dipole.

For the evaluation of (5) and (6), we thus need to calculate the amplitude and the slope of the incident field. For the corresponding analysis, we look at the geometry in Figure 2. The electric or magnetic field produced by a single line current I_e and I_m, respectively, located at $\mathbf{R}'$ is given by [6, eqs. (11-158), (11-170)] and [8, eq. (10.2.6)] according to

$$\begin{aligned} \begin{matrix} E_z^i \\ H_z^i \end{matrix}(\mathbf{R}) &= \begin{matrix} A_{TM} \\ A_{TE} \end{matrix} \frac{1}{2\pi} H_0^{(2)}(k|\,\mathbf{R} - \mathbf{R}'|) \\ &\approx \begin{matrix} A_{TM} \\ A_{TE} \end{matrix} \frac{1+j}{2}\frac{\sqrt{2}}{2\pi^{3/2}}\frac{\exp(-jk|\mathbf{R}-\mathbf{R}'|)}{\sqrt{k|\mathbf{R}-\mathbf{R}'|}} \end{aligned} \tag{7}$$

Note that the approximation in (7) is valid for $k(|\mathbf{R} - \mathbf{R}'|) \gg 1$,that is, in the far field. For the two line currents in Figure 2 of same amplitude but with opposite signs, we thus have in the far field

$$\begin{aligned} \begin{matrix} E_z^i \\ H_z^i \end{matrix}(\mathbf{R}) = \begin{matrix} A_{TM} \\ A_{TE} \end{matrix} \frac{1+j}{2}\pi^{-3/2} \\ \times\left\{\frac{\exp(-jk|\mathbf{R}-\mathbf{R}_1|)}{\sqrt{k|\mathbf{R}-\mathbf{R}_1|}} - \frac{\exp(-jk|\mathbf{R}-\mathbf{R}_2|)}{\sqrt{k|\mathbf{R}-\mathbf{R}_2|}}\right\} \end{aligned} \tag{8}$$

Next, using Taylor expansions we express the two distance terms, which involve $\mathbf{R} - \mathbf{R}_2$ in terms of $\mathbf{R} - \mathbf{R}_1$, and obtain for $|\mathbf{d}| \ll |\mathbf{R} - \mathbf{R_1}|$

$$\begin{aligned} \frac{1}{\sqrt{k|\mathbf{R}-\mathbf{R}_2|}} &= \frac{1}{\sqrt{k|\mathbf{R}-\mathbf{R}_1+\mathbf{d}|}} \\ &= \frac{1}{\sqrt{k\sqrt{|\mathbf{R}-\mathbf{R}_1|^2 + 2\mathbf{d}\cdot(\mathbf{R}-\mathbf{R}_1) + |\mathbf{d}|^2}}} \\ &= \frac{1}{\sqrt{k|\mathbf{R}-\mathbf{R}_1|}\left[1 + 2\frac{\mathbf{d}\cdot(\mathbf{R}-\mathbf{R}_1)}{|\mathbf{R}-\mathbf{R}_1|^2} + \frac{|\mathbf{d}|^2}{|\mathbf{R}-\mathbf{R}_1|^2}\right]^{1/4}} \\ &\simeq \frac{1}{\sqrt{k|\mathbf{R}-\mathbf{R}_1|}}\left[1 - \frac{1}{2}\frac{\mathbf{d}\cdot(\mathbf{R}-\mathbf{R}_1)}{|\mathbf{R}-\mathbf{R}_1|^2}\right] \end{aligned} \tag{9}$$

and

$$k|\mathbf{R}-\mathbf{R}_2| = k|\mathbf{R}-\mathbf{R}_1+\mathbf{d}| = k|\mathbf{R}-\mathbf{R}_1| \times \sqrt{1+2\frac{\mathbf{d}\cdot(\mathbf{R}-\mathbf{R}_1)}{|\mathbf{R}-\mathbf{R}_1|^2}+\frac{|\mathbf{d}|^2}{|\mathbf{R}-\mathbf{R}_1|^2}} \simeq k|\mathbf{R}-\mathbf{R}_1|\left[1+\frac{\mathbf{d}\cdot(\mathbf{R}-\mathbf{R}_1)}{|\mathbf{R}-\mathbf{R}_1|^2}\right] \quad (10)$$

Inserting (9) and (10) into (8) yields at first

$$\begin{matrix}E_z^i\\H_z^i\end{matrix}(\mathbf{R}) = \begin{matrix}A_{TM}\\A_{TE}\end{matrix}\frac{1+j}{2}\pi^{-3/2}\frac{\exp(-jk|\mathbf{R}-\mathbf{R}_1|)}{\sqrt{k|\mathbf{R}-\mathbf{R}_1|}} \times\left[1-\exp\left(-jk\mathbf{d}\cdot\frac{\mathbf{R}-\mathbf{R}_1}{|\mathbf{R}-\mathbf{R}_1|}\right)\left(1-\frac{1}{2}\mathbf{d}\cdot\frac{\mathbf{R}-\mathbf{R}_1}{|\mathbf{R}-\mathbf{R}_1|^2}\right)\right] \quad (11)$$

and finally, because of $|\mathbf{d}| \ll |\mathbf{R}-\mathbf{R_1}|$,

$$\begin{matrix}E_z^i\\H_z^i\end{matrix}(\mathbf{R}) = \begin{matrix}A_{TM}\\A_{TE}\end{matrix}\frac{1+j}{2}\pi^{-3/2}\frac{\exp(-jk|\mathbf{R}-\mathbf{R}_1|)}{\sqrt{k|\mathbf{R}-\mathbf{R}_1|}} \times\left[1-\exp\left(-jk\mathbf{d}\cdot\frac{\mathbf{R}-\mathbf{R}_1}{|\mathbf{R}-\mathbf{R}_1|}\right)\right] \quad (12)$$

For the normal derivative of E_z^i and H_z^i with respect to $\mathbf{R}-\mathbf{R}_1$, we first set $R_1 = 0$ and derive from (12) for $|\mathbf{d}| \ll |\mathbf{R}-\mathbf{R_1}|$

$$\frac{\partial}{\partial\varphi}\begin{matrix}E_z^i\\H_z^i\end{matrix}(\mathbf{R}) = \begin{matrix}A_{TM}\\A_{TE}\end{matrix}\frac{1+j}{2}\pi^{-3/2}\frac{\exp(-jkR)}{\sqrt{kR}} \times\frac{\partial}{\partial\varphi}[1-\exp(-jk\mathbf{d}\cdot\hat{\mathbf{R}})] \quad (13)$$

where $\hat{\mathbf{R}} = \mathbf{R}/R$. With $\hat{\mathbf{R}} = \cos\varphi\hat{\mathbf{x}}+\sin\varphi\hat{\mathbf{y}}$ and $\mathbf{d} = d_x\hat{\mathbf{x}}+d_y\hat{\mathbf{y}}$, we have

$$\begin{aligned}&\frac{\partial}{\partial\varphi}[1-\exp(-jk\mathbf{d}\cdot\hat{\mathbf{R}})]\\&= \frac{\partial}{\partial\varphi}\exp[-jk(d_x\cos\varphi+d_y\sin\varphi)]\\&= (-jk)(-d_x\sin\varphi+d_y\cos\varphi)\exp(-jk\mathbf{d}\cdot\hat{\mathbf{R}})\\&= jk(\mathbf{d}\cdot(\hat{\mathbf{R}}\times\hat{\mathbf{z}})\exp(-jk\mathbf{d}\cdot\hat{\mathbf{R}}).\end{aligned} \quad (14)$$

Because of $\partial n = R\partial\varphi$, we finally obtain for an arbitrary $\mathbf{R}_1$

$$\frac{\partial}{\partial n}\begin{matrix}E_z^i\\H_z^i\end{matrix}(\mathbf{R}) = \begin{matrix}A_{TM}\\A_{TE}\end{matrix}\frac{1+j}{2}\pi^{-3/2}\frac{\exp(-jk|\mathbf{R}-\mathbf{R}_1|)}{\sqrt{k|\mathbf{R}-\mathbf{R}_1|}}\frac{1}{|\mathbf{R}-\mathbf{R}_1|} \times j\,k\,\mathbf{d}\cdot\left(\frac{\mathbf{R}-\mathbf{R}_1}{|\mathbf{R}-\mathbf{R}_1|}\times\hat{\mathbf{z}}\right) \exp\left(-jk\mathbf{d}\cdot\frac{\mathbf{R}-\mathbf{R}_1}{|\mathbf{R}-\mathbf{R}_1|}\right) \quad (15)$$

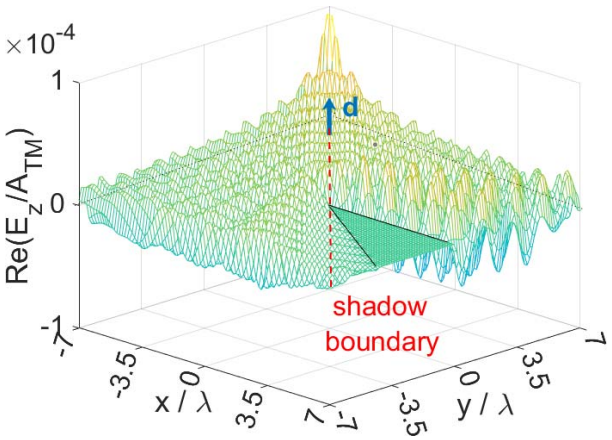

Figure 3. Real part of the normalized total electric field intensity $\mathbf{E} = E_z\hat{\mathbf{z}}$ for a TM-polarized two-dimensional dipole source (with $\mathbf{d}$ polarized in the xy-plane) located at $R' = 10\lambda, \varphi' = 135°$ illuminating a PEC wedge with an outer opening angle $\beta = 330°$. The dipole angle is $\varphi_d = 135°$; that is, the incident field exhibits no slope at the edge. Multipole solution with 100 terms.

4. Numerical Evaluation

As an example, we treat the case of a PEC wedge with an outer opening angle $\beta = 330°$. The two-dimensional dipole source is located at $R' = 10\lambda$ at an angle of incidence $\varphi' = 135°$. To start with an overview, Figure 3 shows the real part of the normalized total electric field intensity (equivalently, the instant value of the time-domain electric field intensity at $t = 0$) for a TM-polarized incident dipole field computed by means of the multipole expansion with a maximum number of 100 terms. This number is determined from the behavior of the Bessel functions for a fixed argument $kR_{\max}$ as a function of the order. To obtain a strictly convergent solution, the maximum order must satisfy $n_{\max} > kR_{\max} + \text{constant}$, where the constant depends on 1) the distance between the radial coordinates of the source and the observation points and 2) the desired accuracy at $R_{\max}$. In the current case, we have $kR_{\max} = 2\pi * 7 * \sqrt{2} \approx 62$; that is, choosing $n_{\max} = 100$ turns out to be sufficient for the entire observation plane. The dipole orientation $\varphi_d = 135°$ leads to an incident field at the edge exhibiting a maximum amplitude but a zero slope. Consequently, if computed by means of the UTD, the field contribution in the sector-like area between the shadow boundary and the wedge ($315° < \phi < 330°$) must come solely from the ordinary diffraction coefficient. In the other areas, the diffraction coefficients also contribute to the total field, which, however, is then dominated by the GO field (i.e., the direct field) and, in the current case for $\varphi < 45°$, the additional reflected field. Consequently, the field in this area is characterized by a strong interference of the direct and the reflected fields.

Figure 4 represents the real part of the normalized total electric field intensity for the case in which the two-dimensional dipole orientation has been turned by

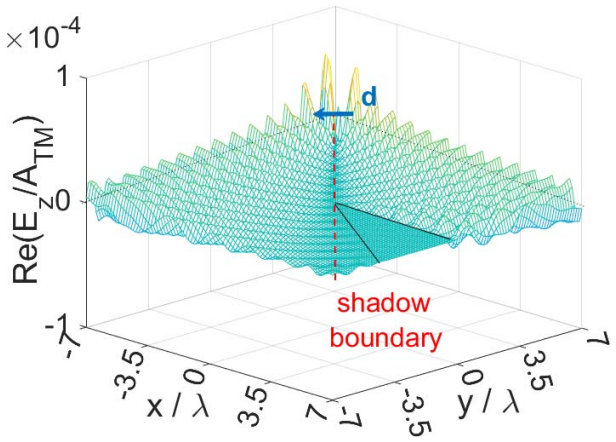

Figure 4. Real part of the normalized total electric field intensity (TM-case; **d** polarized in the *xy*-plane). The dipole angle is $\varphi_d = 45°$; that is, the incident field consists of only a slope and no amplitude at the edge. The other data are as in Figure 3.

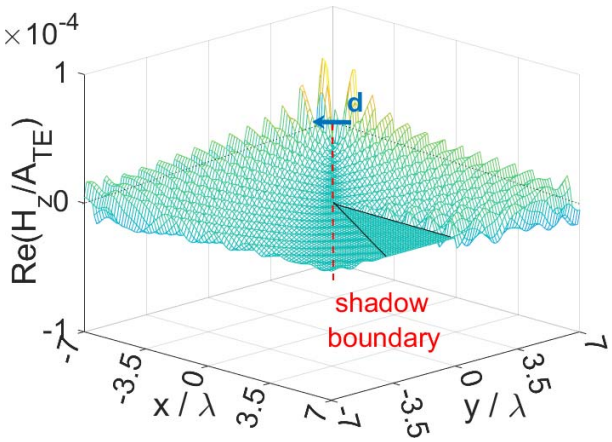

Figure 6. Real part of the normalized total magnetic field intensity (TE-case; **d** polarized in the *xy*-plane). The dipole angle is $\varphi_d = 45°$; that is, the incident field consists of only a slope and no amplitude at the edge. The other data are as in Figure 3.

90°, leading to an incident field at the edge exhibiting a slope only and no amplitude. Thus, if computed by means of the UTD, the field contribution between the shadow boundary and the wedge comes solely from the slope diffraction coefficient.

Figures 5 and 6 show the corresponding snapshots of the magnetic field intensity for the TE case for both the amplitude-only and the slope-only case, respectively. In Figures 7–10, we see comparisons between the exact (multipole) results and the UTD results at different distances from the edge, each as a function of φ for both cases: the no-slope and slope-only incident fields at the edge. Note that both terms, the ordinary as well as the slope diffraction coefficients, have always been employed. We observe a nearly perfect agreement even at very close distances ($R = 0.1\lambda$) to the edge.

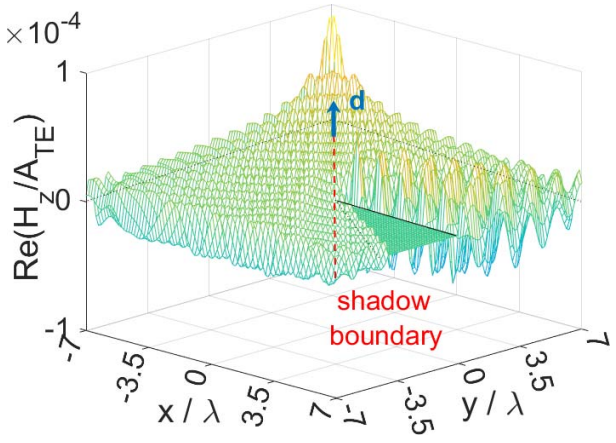

Figure 5. Real part of the normalized total magnetic field intensity (TE-case; **d** polarized in the *xy*-plane). The dipole angle is $\varphi_d = 135°$; that is, the incident field consists of only an amplitude and no slope at the edge. The other data are as in Figure 3.

Finally, Figure 11 shows the case when the incident field includes both an amplitude and a slope. Since we are still nearby the null of the incident field, the slope diffraction contribution is also of importance, as can be seen from the comparison to the case that the slope diffraction contribution has been left out. We observe incorrect results if the slope diffraction has been left out, particularly in the vicinity of the shadow and reflection boundaries.

5. Conclusions

It has been shown that the two-dimensional dipole source is an ideal tool to study the relevance of the

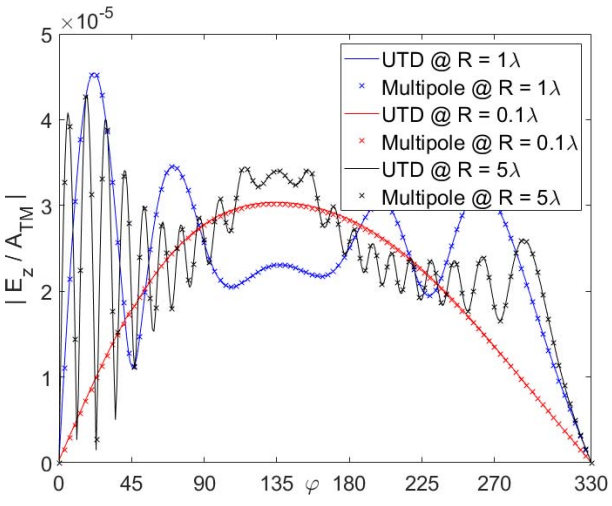

Figure 7. Comparison of the exact total electric field intensity with the corresponding UTD result (TM-case) at three different distances from the edge. The dipole angle is $\varphi_d = 135°$; that is, the incident field consists of only an amplitude and no slope at the edge. The other data are as in Figure 3.

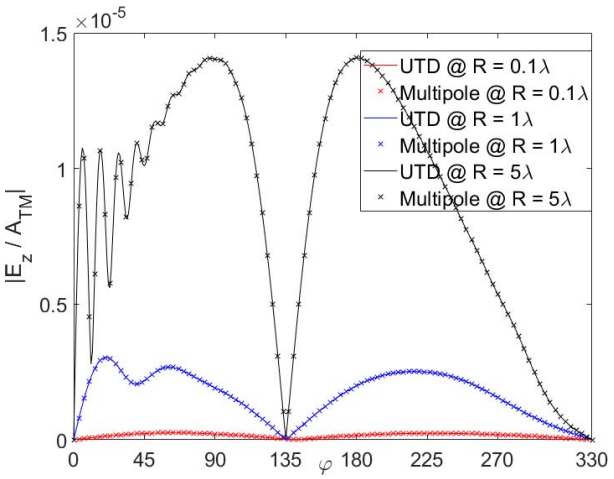

Figure 8. Comparison of the exact total electric field intensities with the UTD result (TM-case) at three different distances from the edge. The dipole angle is $\varphi_d = 45°$; that is, the incident field consists of only a slope and no amplitude at the edge. The other data are as in Figure 3.

slope-diffracted field in certain circumstances. For the evaluation of the incident field, Taylor expansions and asymptotic evaluations have been elaborated for finding closed-form expressions of both the amplitude and the slope. It has been found that the slope-diffracted field can be relevant, particularly for the correct field representation in the shadow region and in the vicinity of the reflection boundary. This is true not only in the case that the incident field consists only of a slope and no amplitude at the edge but also when the incident field exhibits a relatively low amplitude plus a slope at the point of diffraction.

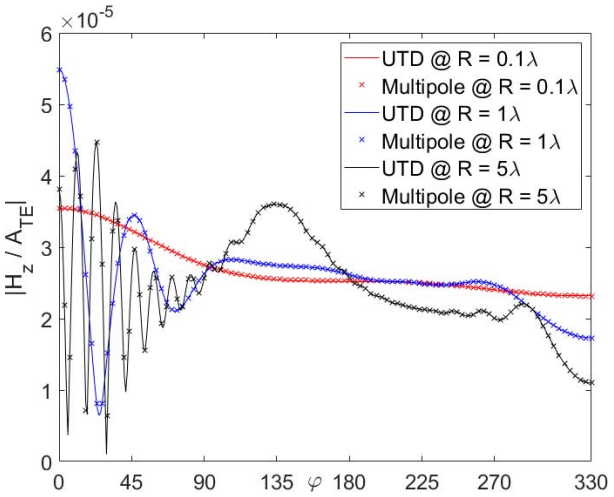

Figure 9. Comparison of the exact total magnetic field intensities with the UTD result (TE-case) at three different distances from the edge. The dipole angle is $\varphi_d = 135°$; that is, the incident field consists of only an amplitude and no slope at the edge. The other data are as in Figure 3.

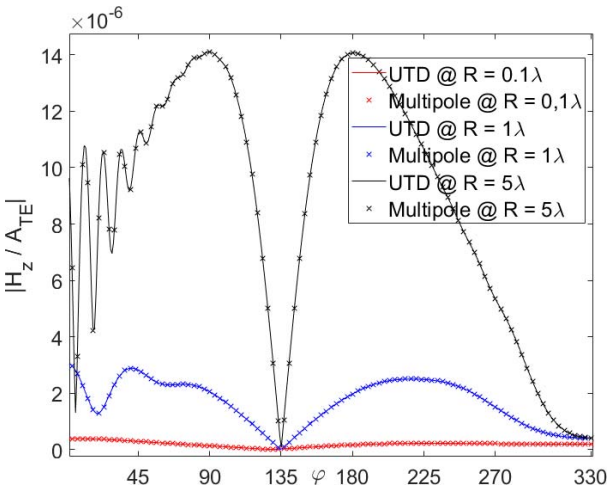

Figure 10. Comparison of the exact total magnetic field intensities with the UTD result (TE-case) at three different distances from the edge. The dipole angle is $\varphi_d = 45°$; that is, the incident field consists of only a slope and no amplitude at the edge. The other data are as in Figure 3.

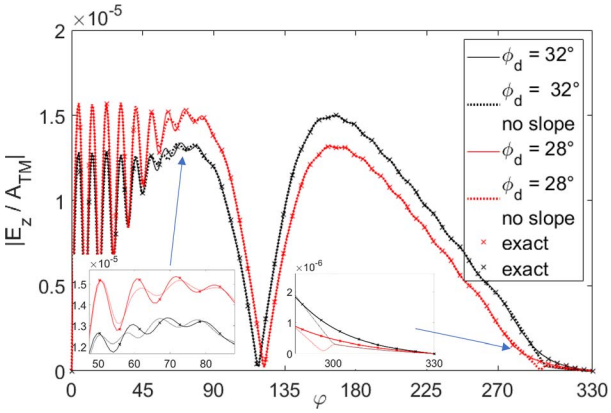

Figure 11. UTD solutions with and without slope-diffraction contributions for a PEC wedge (TM-case) at a distance $R = 5\lambda$ from the edge, including magnifications of the most relevant areas. The two-dimensional dipole source is located at $R' = 10\lambda$, and the angle of incidence is $\varphi' = 120°$. Results are shown for dipole angles $\varphi_d = 28°$ and $\varphi_d = 32°$, that is, slightly off the case of an incident field with only a slope and no amplitude at the edge, which exactly is achieved for $\varphi_d = 30°$.

6. References

1. J. B. Keller, "Geometrical Theory of Diffraction," *Journal of the Optical Society of America*, **52**, 2, February 1962. pp. 116-130.
2. P. H. Pathak, "Techniques for High Frequency Problems," in Y. T. Lo and S. W. Lee (eds.), *Antenna Handbook: Theory, Application and Design*, New York, Van Nostrand Reinhold, 1988.
3. P. H. Pathak and R. J. Burkholder, *Electromagnetic Radiation, Scattering, and Diffraction*, Piscataway, NJ, IEEE Press, 2022.
4. G. Manara and L. Klinkenbusch, "Wedge Diffraction of Fields with a Rapid Spatial Variation of the Amplitude,"

presented at URSI AT/AP RASC 2022, Gran Canaria, Spain, May 29–June 3, 2022.
5. J. J. Bowman, T. B. A. Senior, and P. L. E. Uslenghi (eds.), *Electromagnetic and Acoustic Scattering by Simple Shapes*, New York, Hemisphere Publishing, 1998.
6. C. A. Balanis, *Advanced Engineering Electromagnetics* New York, John Wiley & Sons, 1989.
7. R. Koujoumjian and P. H. Pathak, "A Uniform Geometrical Theory of Diffraction for an Edge in a Perfectly Conducting Surface," *Proceedings of the IEEE*, **62**, 11, November 1974, pp. 1448-1461.
8. National Institute of Standards and Technology, "NIST Digital Library of Mathematical Functions," release 1.1.6, http://dlmf.nist.gov (Accessed March 22, 2023).
9. R. G. Kouyoumjian, T. Celandroni, G. Manara, and P. Nepa, "Inhomogeneous Electromagnetic Plane Wave Diffraction by a Perfectly Conducting Wedge at Oblique Incidence," *Radio Science*, **42**, 2007, p. RS6S06.